

Direct Observation of Quantum Anomalous Vortex in Fe(Se,Te)

Y. S. Lin^{1,*}, S. Y. Wang^{1,*}, X. Zhang², Y. Feng¹, Y. P. Pan¹, H. Ru¹, J. J. Zhu¹, B. K. Xiang¹, K. Liu¹, C. L. Zheng¹, L. Y. Wei², M. X. Wang^{2,3}, Z. K. Liu^{2,3}, L. Chen⁴, K. Jiang⁵, Y. F. Guo², Ziqiang Wang⁶ and Y. H. Wang^{1,7,†}

¹State Key Laboratory of Surface Physics and Department of Physics, Fudan University, Shanghai 200433, China

²School of Physical Science and Technology, ShanghaiTech University, Shanghai 201210, China

³ShanghaiTech Laboratory for Topological Physics, Shanghai 201210, China

⁴Shanghai Institute of Microsystem and Information Technology, Shanghai 200050, China

⁵Institute of Physics, Chinese Academy of Sciences, Beijing 100190, China

⁶Department of Physics, Boston College, Chestnut Hill, Massachusetts 02138, USA

⁷Shanghai Research Center for Quantum Sciences, Shanghai 201315, China



(Received 29 August 2022; revised 8 November 2022; accepted 9 January 2023; published 27 March 2023)

Vortices are topological defects of type-II superconductors in an external magnetic field. In a similar fashion to a quantum anomalous Hall insulator, quantum anomalous vortices (QAV) spontaneously nucleate due to orbital-and-spin exchange interaction between supercurrent and magnetic impurity moment without an external magnetic field. Here, we used scanning superconducting quantum interference device microscopy (sSQUID) to search for its signatures in iron-chalcogenide superconductor Fe(Se,Te). Under zero magnetic field, we found a stochastic distribution of isolated anomalous vortices and antivortices with flux quanta Φ_0 . By applying a small local magnetic field under the coil of the nano-SQUID device, we observed hysteretic flipping of the vortices reminiscent of the switching of ferromagnetic domains, suggesting locally broken time-reversal symmetry. We further observed vectorial rotation of a flux line linking a vortex-antivortex pair by manipulating the local field. These unique properties of the anomalous vortices satisfy the defining criteria of QAV. Our observation suggests an emergent quantum phase with spontaneously nucleated vortex-antivortex matter in an iron-based superconductor with nontrivial topological band structure.

DOI: [10.1103/PhysRevX.13.011046](https://doi.org/10.1103/PhysRevX.13.011046)

Subject Areas: Condensed Matter Physics,
Strongly Correlated Materials,
Superconductivity

I. INTRODUCTION

Vortices are singular phase windings in the complex order parameter of a superconductor. Abrikosov vortices with quantized fluxoid nucleate under an external field H exceeding the lower critical field H_{c1} or when cooling through the critical temperature T_c in a finite H [1]. The magnetic field in the vortex locally breaks time-reversal symmetry (TRS) [Fig. 1(a)], which is a prerequisite for exotic excitations such as isolated Majorana zero modes (MZM) [2–4]. Magnetic impurities break the TRS locally by the exchange coupling to the impurity moment and are

pair breakers in s -wave superconductors. Conventionally, the exchange effects are assumed to suppress the *amplitude* of the superconducting order parameter near the magnetic impurity, creating the celebrated Yu-Shiba-Rusinov (YSR) bound states inside the local superconducting gap.

The situation is very different when there is spin-orbit coupling (SOC). The magnetic moment of the impurity couples to the orbital motion and thus the supercurrent by the spin-orbit exchange coupling, and modulates the *phase* of the superconducting order parameter [5]. For strong enough exchange coupling, it becomes energetically more favorable to generate a spontaneous phase winding equal integer multiples of 2π , i.e., a quantum anomalous vortex (QAV), around the impurity moment compared to the vortex-free state [Fig. 1(a)] [5]. Importantly, the emergence of QAV does not depend on the topological nature of the bulk bands nor the existence of topological surface states. It only requires the strength of the spin-orbit exchange interaction to be larger than the Fermi energy when the superconductor is in the quantum regime [5]. For this reason, QAV is a bulk *vortex* phenomenon, which is

*These authors contributed equally to this work.

†To whom correspondence should be addressed.
wangyhv@fudan.edu.cn

Published by the American Physical Society under the terms of the [Creative Commons Attribution 4.0 International license](https://creativecommons.org/licenses/by/4.0/). Further distribution of this work must maintain attribution to the author(s) and the published article's title, journal citation, and DOI.

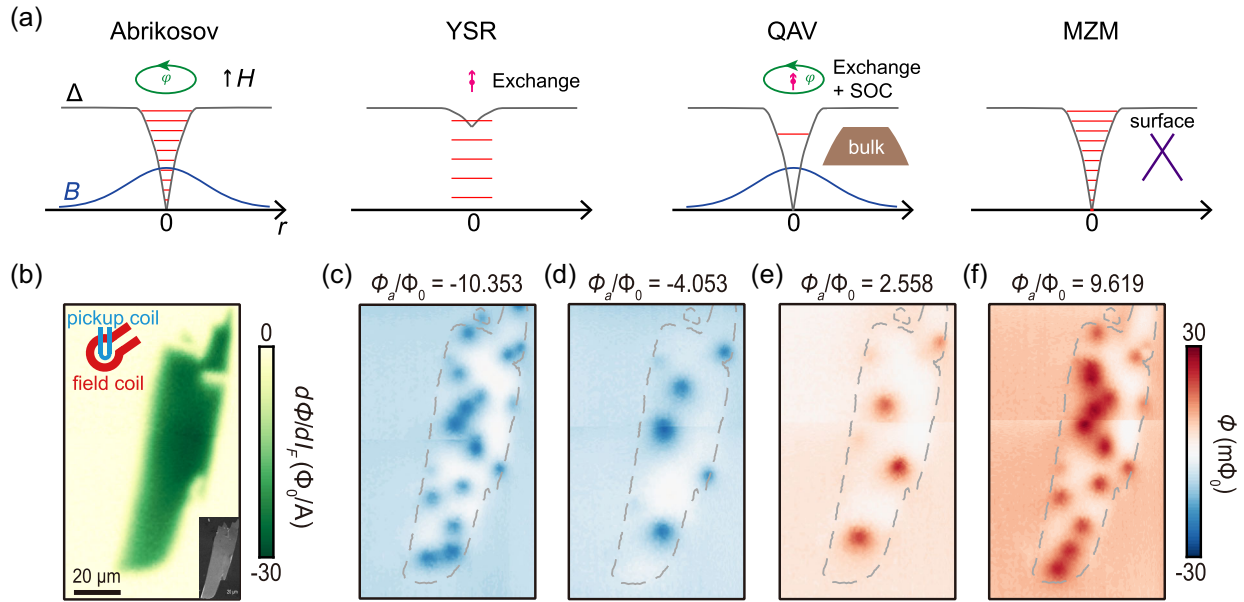


FIG. 1. Abrikosov vortices in an Fe(Se,Te) superconductor imaged by scanning SQUID. (a) Illustration of typical point defects in *s*-wave superconductors. The defects center at $r = 0$. Δ and φ are the amplitude and phase of the superconducting order parameter, respectively, and B is the magnetic induction. Abrikosov: conventional vortex which nucleates with an applied field H ; YSR: Yu-Shiba-Rusinov state, a vortex-free impurity state due to the exchange interaction from the magnetic moment; QAV: quantum anomalous vortex, spontaneous vortex as a result of the exchange interaction from the magnetic impurity and spin-orbit coupling (SOC) from the bulk bands; MZM: Majorana zero mode, a zero-energy charge mode at a vortex core on the Dirac surface states. (b) Susceptometry image of the sample. The dark green area with diamagnetic susceptibility represents the sample, while the white area represents the substrate. The orientation of our SQUID with respect to the sample is illustrated. Inset: scanning electron micrograph of the sample. (c)–(f) Magnetometry images of the sample after field cooling under various applied flux Φ_a through the sample. The gray dashed lines outline the boundary of the sample determined from susceptometry. The horizontal discontinuities in the images were a result of stitching two images together. All the images were obtained at 1.5 K. In this regime of $|\Phi_a| > \Phi_0$, vortices nucleated with the same vorticity as determined by the sign of Φ_a . The amount of observed vortex was clearly larger than $|\Phi_a|/\Phi_0$.

conceptually distinct from the zero-energy *charge* excitation on the superconducting topological surface states embodying MZM.

The namesake of the quantum anomalous vortex matter is the quantum anomalous Hall (QAH) state in a magnetically doped topological insulator [6,7]. In analogy with QAH [8], signatures of QAV are manifestation of the broken TRS as a result of spin-orbital exchange between the impurity moment and vortex supercurrent. For a sufficiently large sample, vortices and antivortices, just like magnetic domains, randomly appear after zero-field cooling; the vorticity of the vortex is determined by the direction of the magnetic moment; vorticity or magnetic moment follows a hysteresis loop under external field sweeps; and the SOC may allow efficient manipulation of the moment by a small current [9–14]. All these defining properties can be used to distinguish spontaneous vortices in superconductors generated quantum mechanically from those that occur thermally.

The iron-chalcogenide superconductor $\text{FeSe}_{0.5}\text{Te}_{0.5}$ (FST) [15–23] is an unconventional superconductor with the essential ingredients for QAV. The YSR state observed on the Fe impurity exhibits spin polarization [24], offering the exchange interaction. It also has small Fermi energy

(4.5 meV) and strong SOC [25–28]. Intriguingly (but nonessential for QAV), FST has shown Z_2 nontrivial topological band structure and superconducting topological surface states [25–28]. Evidence for the zero-energy bound state at a fraction of the magnetic field induced Abrikosov vortices [22,26,27,29–31] and Fe adatoms on the surface of FST [32,33] have been observed by scanning tunneling spectroscopy and interpreted as candidate MZM. However, the direct observation of the QAV, which is intrinsically a flux quantization and vorticity phenomenon in bulk superconductors, has not been made previously. It relies on direct measurements of the quantized magnetic flux of both signs in a zero-field environment and its hysteretic response under a field sweep. All these conditions demand highly sensitive scanning magnetic probes.

II. IMAGING ANOMALOUS VORTICES WITH SCANNING SUPERCONDUCTING QUANTUM INTERFERENCE DEVICE (sSQUID)

Scanning superconducting quantum interference device (sSQUID) microscopy [34–37] is a very sensitive and direct flux-imaging technique. We have installed magnetic shielding around the sample and the SQUID to minimize the

magnitude of the external magnetic field (such as the geomagnetic field). For any residual field after the shielding, which is on the order of milligauss, we used a homemade superconducting coil around the sample to compensate. These procedures allowed us to accurately determine the zero magnetic field condition [38]. The field coil [Fig. 1(b)] on the nano-SQUID [39] can apply a local magnetic field to manipulate a vortex or antivortex without affecting the global vortex structure or suppressing superconductivity.

There were trapped vortices in an FeSe_{0.5}Te_{0.5} flake sample when the applied flux Φ_a was relatively large. We followed the exact same field-cooling and measurement procedure as we did on a conventional superconductor with similar diamagnetic strength which also calibrated the external field and Φ_a [38]. Previous studies showed that the chemical composition and the superconductivity of FST were phase separated into domains hundreds of microns in size [40]. We avoided such inhomogeneity by choosing suitable pieces from the small flake samples after exfoliation. Since the diamagnetic susceptibility was directly proportional to superfluid density, the uniformity in susceptometry [Fig. 1(b)] showed superconducting homogeneity of our sample. Our extensive sample characterizations at different length scales also suggested uniform superconductivity up to the sample size [38]. We cooled the FST sample from 18 to 1.5 K through its $T_c \sim 14$ K at a cooling rate of 50 mK/s to prevent any thermally excited vortex-antivortex pairs from freezing [41]. We applied a fixed Φ_a during cooling and scanning microscopy and repeated the process for various Φ_a 's. In the regime of $|\Phi_a| > \Phi_0$, where $\Phi_0 = h/2e$ (h is the Planck constant and e is the electron charge) is the superconducting flux quantum, we obtained the magnetometry images showing trapped vortex throughout the sample [Figs. 1(c)–1(f)]. These vortices exhibited the same vorticity determined by the sign of Φ_a . This situation seemed similar to that of a conventional superconductor (Fig. S6 in Supplemental Material [38]) except that the number of observed vortices was clearly larger than $|\Phi_a|/\Phi_0$ in FST. The average value and the spread of the width of the vortices were very similar to those of vortices on the Nb film (Fig. S11 [38]). This fact was a further testament of the superconducting homogeneity of the FST samples and suggested that large fields predominantly induced Abrikosov vortices.

Surprising vortex patterns appeared when $|\Phi_a| < \Phi_0$, the low-field regime where no vortex was expected or observed on a conventional superconductor (Fig. S6 [38]). We performed 27 field-cooling cycles in this regime on this particular FST sample [38]. The magnetometry images were drastically different even if Φ_a was changed slightly and we present here some representative images [Figs. 2(a)–2(f)]. Vortices of both vorticity showed up simultaneously within the same image even for finite Φ_a [Figs. 2(a)–2(c)]. At calibrated zero field, the images were different each time: in some cases, no vortex was observed [Fig. 2(d)], while in others vortices and antivortices

appeared at random locations [Figs. 2(e) and 2(f)]. The fact that the zero-vortex state did occur ruled out thermally induced vortex-antivortex, which always generated the same density of pairs at a fixed quenching rate [41]. Regardless of vorticity, isolated vortices showed total flux of Φ_0 [Figs. 2(a), 2(b), and 2(f)]. We have observed a similar effect in all the FST samples we fabricated with similar composition [38]. An isolated vortex was possible under zero-field cooling for finite-sized samples because the flux line can loop back outside the sample.

The FST samples we used contained a dilute amount of interstitial Fe (<1%) to act as impurity magnetic moments. At such low concentration, the impurity moments did not form long-range magnetic order [12–15]. Nevertheless, chemical or crystalline inhomogeneities may cause flux trapping in even a well-shielded low-field environment. For these reasons, we carried out similar zero-field cooling and measurements in the same setup in different types of control samples: Fe(2 nm)/Nb(80 nm), FeSe without the Te alloying, and Fe_{1+y}(Se, Te) with a much higher concentration (nominally $\sim 10\%$) of interstitial Fe impurity [38]. Since these control samples had either nominally similar or higher impurity density than FST, they further ruled out conventional pinning due to sample inhomogeneity [42,43] or instrumental artifact. The absence of vortex in FST above T_c ruled out magnetic clustering. These control experiments suggest that the stochastic occurrence of spontaneous vortices and antivortices with quantized flux under zero magnetic field was an intrinsic effect of FST with low interstitial Fe.

The number of vortices and antivortices from all these cooling cycles gave us statistical insights of the peculiar random vortex patterns. When $|\Phi_a| < \Phi_0$, the number of vortices or antivortices in FST fluctuated toward both sides in similar amplitudes against a flat baseline from the Nb control sample [Fig. 2(g)]. However, as $|\Phi_a|$ got bigger, there was a positive correlation between Φ_a and the number of vortices with the same sign as Φ_a . Although the probability of observing antivortices quickly diminished when $|\Phi_a| \gtrsim \Phi_0$, the number of observed vortices still fluctuated. The total number of observed vortices was much higher than $|\Phi_a|/\Phi_0$ [Fig. 2(g), black dashed line], whereas the number of Abrikosov vortices in Nb was lower. Such behavior was consistent with a positive bulk magnetization below T_c under field cooling of FST with magnetic impurities [see, e.g., Fig. 1(c) in Ref. [23]]. The generation of more flux than what was applied suggested ferromagnetic exchange interaction from the magnetic impurity moment, such as that of the excess Fe ions.

Having established the existence of anomalous vortex and its connection with magnetic impurity, we study the flux profiles of spontaneous vortex-antivortex duos to understand the origin of randomness. Duos which located close to each other [Figs. 2(a), 2(c), and 2(f), arrows] showed quite different contrast and shape from the isolated ones [Figs. 2(a), 2(b), and 2(f), dashed circles]. The line

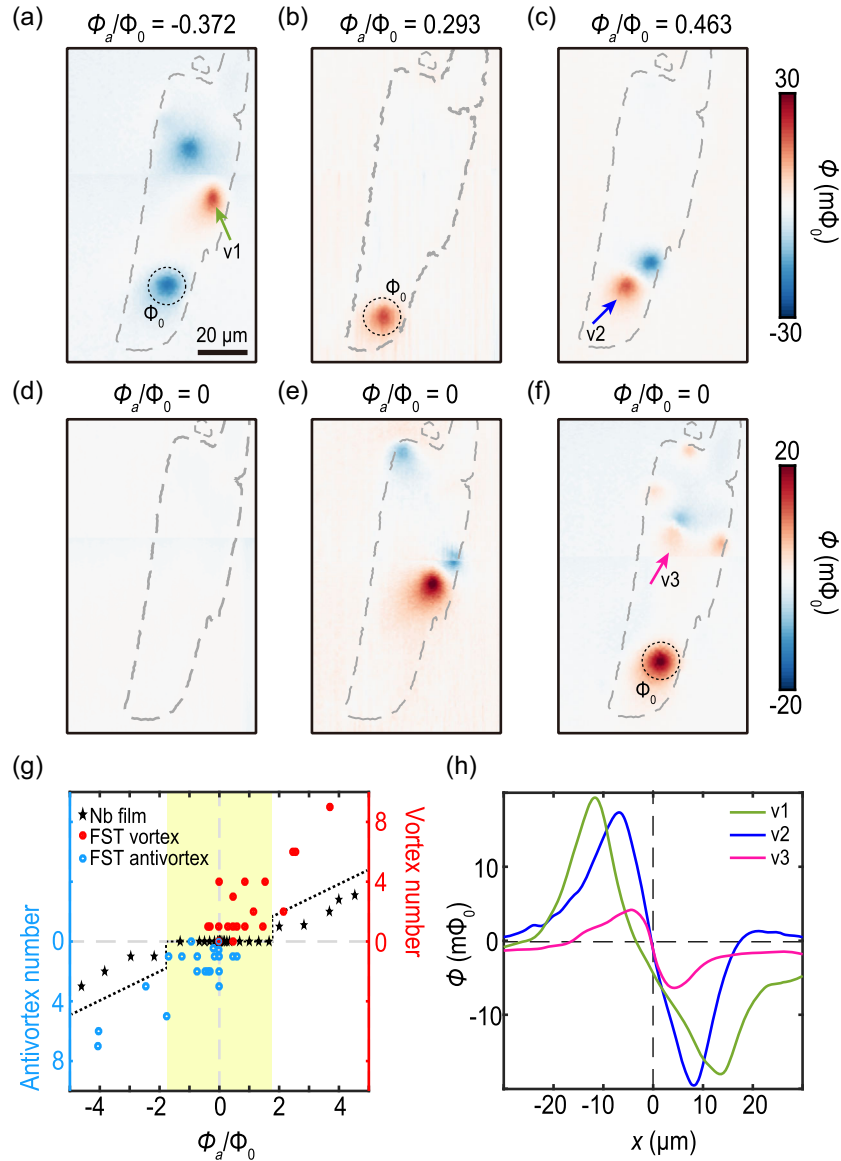


FIG. 2. Spontaneous generation of quantum anomalous vortex in Fe(Se,Te) under zero-field cooling. (a)–(f) Magnetometry images of the sample after field cooling under various $|\Phi_a| < \Phi_0$, a regime no vortex was expected to exist on a conventional superconductor. They are representatives of the 27 images obtained in this regime. In the strict zero-field cooling cases (d)–(f), the vortex-antivortex patterns appeared different each time (more in Ref. [38]). Dashed circles in (d), (b), and (f) outline isolated vortices with quantized flux of Φ_0 . (g) Number of vortices as a function of Φ_a . The red dots and blue circles represent positive and negative vortex number, respectively, under each cooling case, while the black stars were a baseline from the Nb film [Fig. S5(k) in Supplemental Material [38]]. The yellow shaded area represents the low-field regime where no vortex was observed on Nb while spontaneous vortices appeared in Fe(Se,Te). The black dashed line outside the low-field regime marks the boundary where the vortex number equals Φ_a/Φ_0 . The random and spontaneous vortex formations of both vorticities suggest the nucleation of QAV and antivortex. (h) Line cuts of three typical vortex-antivortex patterns. The three cuts (green, cyan, and magenta) are along the arrow directions v1, v2, and v3 in (a), (c), and (f) with matching colors, respectively. The coupling between QAV-antivortex was stronger when they located closer.

cuts through the duos showed that the peak-to-peak flux reduced with decreasing distances [Fig. 2(h)]. The farthest duo (noted as v1) has about $0.9 \Phi_0$ per vortex and looked like two monopoles with opposite signs [Fig. 2(a)]. The closest duo (v3) amounts to only $0.15 \Phi_0$ per vortex and appeared as a magnetic dipole [Fig. 2(h)]. Out of the 27 images, there were 6 discernable cases of v3 [38]. The

variation in the shape of the duo could be understood when considering the magnetic energy of the flux line. The decay length we observed of a typical isolated vortex was around $10 \mu\text{m}$ [Fig. 2(b)], consistent with the expected Pearl length $\Lambda = (2\lambda^2/d)$, where $\lambda \sim 500 \text{ nm}$ was the London penetration depth of bulk FST and $d \sim 100 \text{ nm}$ [38] was the thickness of our sample. When the pair separation was

larger than Λ , there was little magnetic interaction between the vortex and antivortex. The flux lines through them were mostly normal at the surface, bending to connect far away from the sample. The quantized flux captured by sSQUID close to the surface was thus hardly affected by the other and the duo assembled into a double-monopole pattern. As the separation got smaller, it costed more energy for the flux lines to bend around a “U turn.” As a result, the flux lines tilted toward each other slightly at the surface to reduce the bend, which led to reduced flux along the surface normal (v2). When the separation was further reduced (v3), the flux lines tilted heavily toward each other to minimize the magnetic energy. This diminished the flux along the surface normal and the flux of the vortex appeared $\ll \Phi_0$. Since the average distance between interstitial Fe ions [18], through which vortex or antivortex resided, was much smaller than Λ , most of the duos canceled each other out on the mesoscopic scale. Those that were detected happened because the two properly separated vortex and antivortex were not paired up by

others that were much closer. This process of pair making from a statistically large amount of impurity centers led to the stochastic nature of the anomalous vortex patterns.

III. HYSTERETIC SWITCHING OF THE VORTEX-ANTIVORTEX PAIR

In order to study the switching of vortex-antivortex pair under magnetic field, we focused on a different FST sample (Fig. 3). After zero-field cooling, this sample had a higher probability of forming a double-dipole-like pattern in its lower section [Fig. 3(a), inset], likely due to its particular shape. To tune the moments of the vortices without affecting other parts of the sample, we applied a local magnetic field H_F by passing a current through the field coil on our nano-SQUID [Fig. 3(a)]. Before each scan, we moved the field coil over to the middle of the duo and applied a particular H_F as labeled above the images. Then, we turned off H_F before acquiring the magnetometry image. Each image [Figs. 3(a)–3(j)] was obtained in this

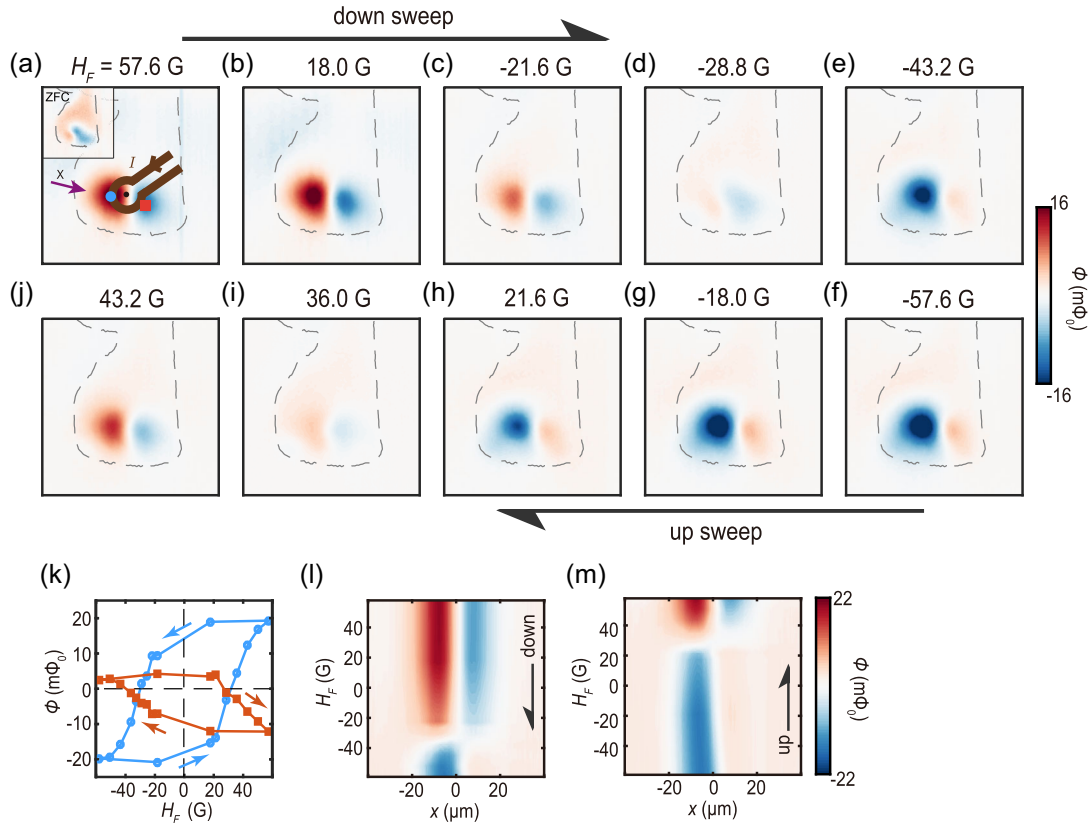


FIG. 3. Hysteretic switching of QAV and its antivortex using a local field. (a)–(j) Magnetometry images of an Fe(Se,Te) sample obtained at 1.5 K and zero field. The dashed lines outline the shape of the sample as obtained from susceptometry. A local field H_F is applied by passing a dc current through the field coil [(a), brown line] on the nano-SQUID probe at the middle of the vortex-antivortex dual [(a), black dot] and then removed before each image was taken. The history of the images is indicated by the black arrows showing field sweeping directions. (a) Inset: image after zero-field cooling (ZFC) and before applying any H_F . (k) Flux signals extracted from the two points [(a), blue dot and orange square] as a function of H_F . The magnetic hysteresis loops exhibiting opposite winding with H_F correspond to QAV and antivortex, respectively. (l), (m) Interpolated images from the line cuts through the pattern in (a) (arrow direction) as a function of H_F from down and up sweeps, respectively. The hysteresis in the switching was reminiscent of a ferromagnetic magnetization loop and suggested spontaneously broken time-reversal symmetry.

manner following the sequence of “down sweep” and then “up sweep,” completing a loop. Starting from $H_F = 57.6$ G [Fig. 3(a)], we observed a much stronger single-dipolar pattern consistent with the vortex-antivortex pair in other samples [Fig. 2(c)]. As the applied H_F decreased, the contrast of the dipole reduced at $H_F = 18$ G [Fig. 3(b)] but kept the same sign even after a negative $H_F = -21.6$ G was applied [Fig. 3(c)]. When $H_F = -28.8$ G, the pattern [Fig. 3(d)] became very similar to the initial one before any H_F was applied [Fig. 3(a) inset]. Further sweeping down to $H_F = -43.2$ G [Fig. 3(e)] and $H_F = -57.6$ G [Fig. 3(f)], we finally obtained a reversed vortex-antivortex pattern from the one in $H_F = 57.6$ G [Fig. 3(a)]. The up-sweep images [Figs. 3(f)–3(j)] were just the opposite of the down-sweep images, where reversal appeared at $H_F = 36$ G [Fig. 3(i)]. The pattern we obtained after cycling back to $H_F = 57.6$ G (not shown) was exactly the same as the original one. It was clear from the above sequence that the vorticities of the vortex and antivortex under a local field were history dependent.

The hysteresis in the switching was better visualized in a flux-field diagram [Fig. 3(k)]. The trajectories followed by the vortex and the antivortex followed opposite winding directions with respect to the field sweep. The flux of both loops reversed signs after the field switched directions. By combining the line cuts through the dipole taken from magnetometry images at various H_F of the down sweep [Fig. 3(l)] and that of the up sweep [Fig. 3(m)], we found that the vortex and antivortex switched their signs concurrently. Such synchronous inversion of their vorticity suggested that they were paired by threading a common flux tube through both impurity moments. Conventional vortices with pinning also exhibit hysteresis in the magnetization-field curve. However, the magnetization typically reverses sign before the field ramps down to zero [1,44–46]. Instead, our anomalous vortex loops were reminiscent of a magnetization-field hysteresis loop of a ferromagnet. (Note that the reversal fields were not as sharp as a typical coercive field of a hard ferromagnet largely because the local field H_F had to be removed during scanning imaging to avoid scrambling the structure.) The ferromagnetlike hysteresis loop strongly suggested spontaneous TRS breaking. The anomalous vortex and antivortex we observed satisfied all the signatures of QAV.

IV. VECTORIAL ROTATION OF FLUX LINE

The magnitude and polarities of the pair revealed vectorial rotation of magnetic impurities moments under the application of H_F . The total flux of the vortex (antivortex) was $1.0 \Phi_0$ ($-0.6 \Phi_0$) when the contrast reached its maximum at $H_F = 57.6$ G [Fig. 3(a)], whereas that at the reversal field $H_F = -28.8$ G [Fig. 3(d)] was $0.1 \Phi_0$ ($-0.2 \Phi_0$). These values corresponded to cases v2 and v3 pairs, respectively, and suggested that they had an in-plane component. The fact that the total flux of the pair did not sum to zero suggested that the moments in the

vortex cores were not antiparallel. The tilting from the surface normal into the plane was most obvious when the pair had the least out-of-plane component, which happened at the reversals. The images we obtained at $H_F = -28.8$ G during the down sweep [Fig. 4(a)] and $H_F = 36$ G during the up sweep [Fig. 4(b)] showed qualitatively similar patterns as that from zero-field cooling [Fig. 3(a), inset]. They both consisted of two dipoles aligned off axis and their polarities followed the same “minus-plus, minus-plus” order clockwise [Fig. 4(c)]. The characteristic H_F is an order of magnitude smaller than the H_{C1} of FST at 3 K [38] and thus not capable of generating or annihilating an Abrikosov vortex. The Meissner current induced by such a small local magnetic field exerts a Lorentz force on an existing Abrikosov vortex and causes some lateral displacement [47]. However, the double-dipolar pattern and the hysteretic switching were both inconsistent with a lateral displacement of the original structure.

Remarkably, each single-dipolar pattern agrees well with the theoretical calculations of a single QAV nucleated at a magnetic impurity carrying a local moment canted away from the normal of the surface [38]. To simulate the out-of-plane field in the above configuration, we combined the calculated current distributions of isolated QAV and antivortex with in-plane moments [38] and computed the out-of-plane field measured by sSQUID using Biot-Savart law [Fig. 4(d)]. For such a crude model without explicitly including the vortex-antivortex interaction, it showed qualitative agreement with the measured patterns [Figs. 4(a) and 4(b)]. The agreement suggested that the Meissner current J_F induced by H_F was driving a vectorial rotation of the coupled spin-flux line [Fig. 4(e)]. We speculate that the driving mechanism is similar to current-induced torque in magnetic metals with SOC [48,49]. This is based on the observed vector product relation between the in-plane flux and $\mathbf{J}_F \times \mathbf{S}$, where \mathbf{S} is the impurity moment, on both the vortex and antivortex [Fig. 4(d)]. Since \mathbf{J}_F was absent during imaging, the presence of in-plane configuration suggested it was a metastable state, which explains why it also occurred after zero-field cooling [Fig. 3(a)]. The hysteresis in the switching H_F [Figs. 3(k)–3(m)] then reflects that the applied torque has to overcome a potential from the supercurrent of the vortices to first reach the in-plane configuration, at which point \mathbf{J}_F and the vortex supercurrent align at the vortex-antivortex cores [Fig. 4(d) herein and Fig. S13 in Supplemental Material [38]]. This sequence of vortex-antivortex pair rotation by small H_F is a manifestation of the interaction between the impurity spin and the supercurrent, which is the quantum origin of QAV.

The emergent behavior of the QAV was a local effect in the low excess Fe impurity (<1%) samples we measured. In this dilute regime, the vortex cores were still well separated and the broken TRS determined by exchange interaction length was several lattice sites around the impurity [50]. Formation of vortex-antivortex was more favorable than parallel alignments of the moments due to the lower free

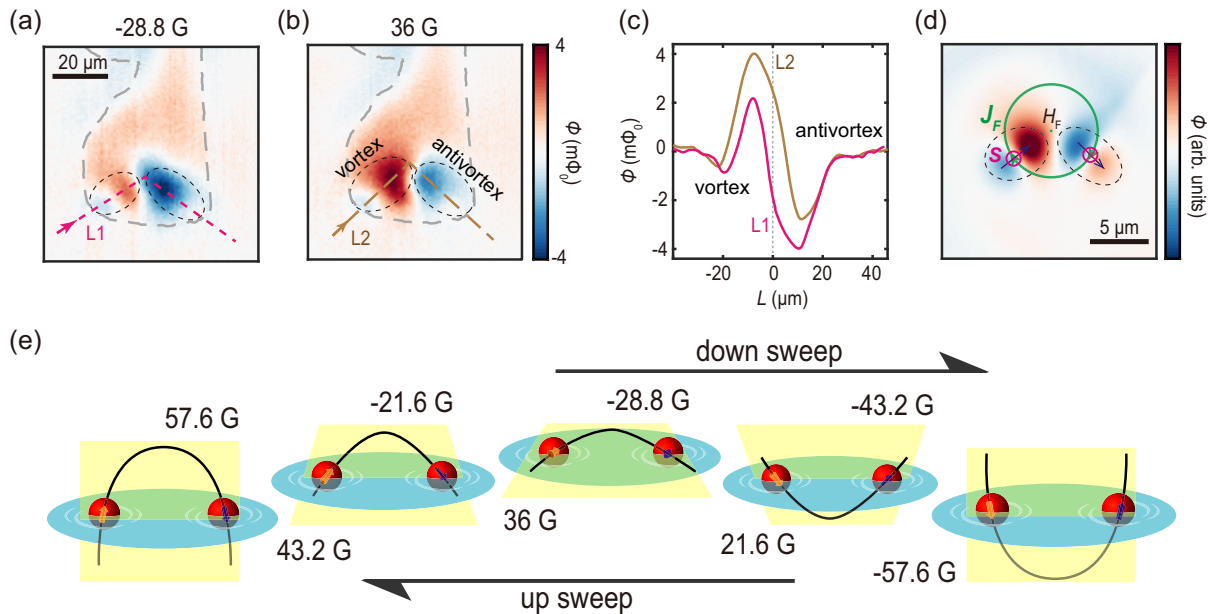


FIG. 4. Vectorial rotation of a QAV and its antivortex. (a),(b) Magnetometry images from Figs. 3(d) and 3(i), respectively, rescaled in color. (c) Line profiles from (a) and (b) along the dashed lines. The origin is set to the center of the field coil. (d) Simulated out-of-plane magnetic field of a QAV-antivortex pair oriented in plane (see text). The local field H_F induces a Meissner current \mathbf{J}_F , which points at different directions at the cores of the vortex and the antivortex. Their impurity moments \mathbf{S} also orient oppositely. The torque from the cross product $\mathbf{J}_F \times \mathbf{S}$ generates the in-plane spin component (purple arrows). (e) Illustration depicting a pair and its impurity (red spheres) moments (orange and purple arrows) rotating about their central axis when a local field was applied. The blue circular plate represents the sample in plane; the black line represents the flux line which goes through the impurity moments; the yellow plane is an auxiliary plane the moments and the flux line are confined to. The fields match the corresponding fields in Figs. 3(a)–3(j). Such polar rotations of the flux line of QAV differentiated it from horizontal motion of an Abrikosov vortex by a local probe and suggested a new mechanism enabling efficient manipulation of vortex.

energy of the pair. Lowering the Fe impurity would reduce the probability of finding the QAV. On the other hand, increasing the Fe impurity density would decrease their average distance to be much smaller than the coherence length so that the vortex cores would start to overlap heavily [23]. They might develop collective long-range ferromagnetic order by a Ruderman–Kittel–Kasuya–Yosida-like interaction through the assistance of SOC and supercurrents [51,52]. A more quantitative analysis is required to elucidate this strong-interaction regime at sufficiently high excess Fe concentrations, in connection to the observed gapping of the Dirac point associated with the topological surface states [53]. The evolution of QAV with the impurity concentration is outside the scope of the current work and may be systematically examined by both volumetric and local techniques in the future. With sufficient impurity moments, it may be possible to drive and detect ferromagnetic resonance of the moments using a high frequency alternate current through the sample.

The magnetic impurity induced topological vortex matter we observed may be harnessed for quantum information technology [54–59]. Because FST has shown a Z_2 non-trivial topological band structure and superconducting topological surface states [25–28], both its Abrikosov vortices and the QAVs support degenerate zero-energy

excitations or MZM, which are anyons that obey non-Abelian statistics [54–56]. Fusion and braiding of such an anionic vortex with its antiparticle are essential for fault-tolerant quantum computation [57,58]. Since free Abrikosov vortices typically have the same vorticity and thus repel each other, it will be difficult to annihilate them in order to fuse the MZM without destroying the superconducting condensate. The perturbative nature of our local field avoids collapsing the superconducting gap and protects adiabaticity during manipulation [54,55]. Additional braiding schemes are also possible by bringing a free Abrikosov vortex around QAV-antivortex pairs using similar sSQUID manipulations.

In conclusion, we used sSQUID microscopy and directly observed a novel form of vortex with spontaneously broken TRS in Fe-based superconductor Fe(Se,Te). QAVs and its antivortices occurred stochastically at zero magnetic field due to the SOC between the impurity moment and the supercurrent. By applying a small local magnetic field from the nano-SQUID probe, we observed ferromagneticlike hysteretic switching loops, following a vectorial rotation of the flux line threading the impurity spin. Our observation and manipulation of QAV may enable new possibilities for superconducting information technology in a promising material platform.

ACKNOWLEDGMENTS

Y. H. W. would like to acknowledge support by NSFC Grants No. 11827805 and No. 12150003, National Key R&D Program of China Grant No. 2021YFA1400100, and Shanghai Municipal Science and Technology Major Project Grant No. 2019SHZDZX01. Y. F. G. would like to acknowledge support by NSFC Grant No. 11874264. Z. W. is supported by U.S. DOE, Basic Energy Sciences Grant No. DE-FG02-99ER45747. C. L. Z. and K. L. acknowledge the financial support from NSFC Grant No. 61871134 and Shanghai Municipal Science and Technology Commission Grant No. 18JC141030. Z. K. L. would like to acknowledge support by the National Key R&D program of China Grant No. 2017YFA0305400. All the authors are grateful for the stimulating discussions with Y. Yu, J. Shen, X. Dai, and J. Zi, as well as experimental assistance by J. Zhao, D. Jiang, T. Zhang, and D. L. Feng. The data that support the findings of this work are available from the corresponding author upon reasonable request.

-
- [1] M. Tinkham, *Introduction to Superconductivity* (McGraw-Hill, New York, 1996).
- [2] C. Kallin and J. Berlinsky, *Chiral Superconductors*, *Rep. Prog. Phys.* **79**, 054502 (2016).
- [3] X.-L. Qi and S.-C. Zhang, *Topological Insulators and Superconductors*, *Rev. Mod. Phys.* **83**, 1057 (2011).
- [4] M. Z. Hasan and C. L. Kane, *Colloquium: Topological Insulators*, *Rev. Mod. Phys.* **82**, 3045 (2010).
- [5] K. Jiang, X. Dai, and Z. Wang, *Quantum Anomalous Vortex and Majorana Zero Mode in Iron-Based Superconductor Fe(Te, Se)*, *Phys. Rev. X* **9**, 0011033 (2019).
- [6] R. Yu, W. Zhang, H. J. Zhang, S. C. Zhang, X. Dai, and Z. Fang, *Quantized Anomalous Hall Effect in Magnetic Topological Insulators*, *Science* **329**, 61 (2010).
- [7] C. Z. Chang *et al.*, *Experimental Observation of the Quantum Anomalous Hall Effect in a Magnetic Topological Insulator*, *Science* **340**, 167 (2013).
- [8] W. Wang, Y. Ou, C. Liu, Y. Wang, K. He, Q.-K. Xue, and W. Wu, *Direct Evidence of Ferromagnetism in a Quantum Anomalous Hall System*, *Nat. Phys.* **14**, 791 (2018).
- [9] V. M. Edelstein, *Magnetoelectric Effect in Polar Superconductors*, *Phys. Rev. Lett.* **75**, 2004 (1995).
- [10] M. Smidman, M. B. Salamon, H. Q. Yuan, and D. F. Agterberg, *Superconductivity and Spin-Orbit Coupling in Non-Centrosymmetric Materials: A Review*, *Rep. Prog. Phys.* **80**, 036501 (2017).
- [11] S. S. Pershoguba, K. Björnson, A. M. Black-Schaffer, and A. V. Balatsky, *Currents Induced by Magnetic Impurities in Superconductors with Spin-Orbit Coupling*, *Phys. Rev. Lett.* **115**, 116602 (2015).
- [12] F. S. Bergeret and I. V. Tokatly, *Theory of the Magnetic Response in Finite Two-Dimensional Superconductors*, *Phys. Rev. B* **102**, 060506(R) (2020).
- [13] S. K. Yip, *Two-Dimensional Superconductivity with Strong Spin-Orbit Interaction*, *Phys. Rev. B* **65**, 144508 (2002).
- [14] J. J. He, K. Hiroki, K. Hamamoto, and N. Nagaosa, *Spin Supercurrent in Two-Dimensional Superconductors with Rashba Spin-Orbit Interaction*, *Commun. Phys.* **2**, 128 (2019).
- [15] F.-C. Hsu *et al.*, *Superconductivity in the PbO-Type Structure α -FeSe*, *Proc. Natl. Acad. Sci. U.S.A.* **105**, 14262 (2008).
- [16] M. H. Fang, H. M. Pham, B. Qian, T. J. Liu, E. K. Vehstedt, Y. Liu, L. Spinu, and Z. Q. Mao, *Superconductivity Close to Magnetic Instability in Fe(Se_{1-x}Te_x)_{0.82}*, *Phys. Rev. B* **78**, 224503 (2008).
- [17] B. C. Sales, A. S. Sefat, M. A. McGuire, R. Y. Jin, D. Mandrus, and Y. Mozharivskyj, *Bulk Superconductivity at 14 K in Single Crystals of Fe_{1+y}Te_xSe_{1-x}*, *Phys. Rev. B* **79**, 094521 (2009).
- [18] Y. Sun, T. Yamada, S. Pyon, and T. Tamegai, *Influence of Interstitial Fe to the Phase Diagram of Fe_{1+y}Te_xSe_{1-x} Single Crystals*, *Sci. Rep.* **6**, 32290 (2016).
- [19] N. Hao and J. Hu, *Special Topic: Topological Matter: Topological Quantum States of Matter in Iron-Based Superconductors: From Concept to Material Realization*, *Natl. Sci. Rev.* **6**, 213 (2019).
- [20] B. Jäck, Y. Xie, J. Li, S. Jeon, B. A. Bernevig, and A. Yazdani, *Observation of a Majorana Zero Mode in a Topologically Protected Edge Channel*, *Science* **364**, 1255 (2019).
- [21] M. J. Gray *et al.*, *Evidence for Helical Hinge Zero Modes in an Fe-Based Superconductor*, *Nano Lett.* **19**, 4890 (2019).
- [22] T. Machida, Y. Sun, S. Pyon, S. Takeda, Y. Kohsaka, T. Hanaguri, T. Sasagawa, and T. Tamegai, *Zero-Energy Vortex Bound State in the Superconducting Topological Surface State of Fe(Se, Te)*, *Nat. Mater.* **18**, 811 (2019).
- [23] D. Jiang *et al.*, *Observation of Robust Edge Superconductivity in Fe(Se, Te) under Strong Magnetic Perturbation*, *Sci. Bull.* **66**, 425 (2021).
- [24] D. Wang, J. Wiebe, R. Zhong, G. Gu, and R. Wiesendanger, *Spin-Polarized Yu-Shiba-Rusinov States in an Iron-Based Superconductor*, *Phys. Rev. Lett.* **126**, 076802 (2021).
- [25] Z. Wang *et al.*, *Topological Nature of the FeSe_{0.5}Te_{0.5} Superconductor*, *Phys. Rev. B* **92**, 115119 (2015).
- [26] X. Wu, S. Qin, Y. Liang, H. Fan, and J. Hu, *Topological Characters in Fe(Te_{1-x}Se_x) Thin Films*, *Phys. Rev. B* **93**, 115129 (2016).
- [27] G. Xu, B. Lian, P. Tang, X.-L. Qi, and S.-C. Zhang, *Topological Superconductivity on the Surface of Fe-Based Superconductors*, *Phys. Rev. Lett.* **117**, 047001 (2016).
- [28] P. Zhang *et al.*, *Observation of Topological Superconductivity on the Surface of an Iron-Based Superconductor*, *Science* **360**, 182 (2018).
- [29] M. Chen, X. Chen, H. Yang, Z. Du, X. Zhu, E. Wang, and H.-H. Wen, *Discrete Energy Levels of Caroli-de Gennes-Matricon States in Quantum Limit in FeTe_{0.55}Se_{0.45}*, *Nat. Commun.* **9**, 970 (2018).
- [30] D. Wang *et al.*, *Evidence for Majorana Bound States in an Iron-Based Superconductor*, *Science* **362**, 333 (2018).
- [31] L. Fu and C. L. Kane, *Superconducting Proximity Effect and Majorana Fermions at the Surface of a Topological Insulator*, *Phys. Rev. Lett.* **100**, 096407 (2008).

- [32] J.-X. Yin *et al.*, *Observation of a Robust Zero-Energy Bound State in Iron-Based Superconductor Fe(Te, Se)*, *Nat. Phys.* **11**, 543 (2015).
- [33] P. Fan *et al.*, *Observation of Magnetic Adatom-Induced Majorana Vortex and Its Hybridization with Field-Induced Majorana Vortex in an Iron-Based Superconductor*, *Nat. Commun.* **12**, 1348 (2021).
- [34] J. R. Kirtley and J. P. Wikswo, *Scanning SQUID Microscopy*, *Annu. Rev. Mater. Sci.* **29**, 117 (1999).
- [35] J. R. Kirtley, *Fundamental Studies of Superconductors Using Scanning Magnetic Imaging*, *Rep. Prog. Phys.* **73**, 126501 (2010).
- [36] T. Nishio, V. H. Dao, Q. Chen, L. F. Chibotaru, K. Kadowaki, and V. V. Moshchalkov, *Scanning SQUID Microscopy of Vortex Clusters in Multiband Superconductors*, *Phys. Rev. B* **81**, 020506(R) (2010).
- [37] P. Reith and H. Hilgenkamp, *Analysing Magnetism Using Scanning SQUID Microscopy*, *Rev. Sci. Instrum.* **88**, 123706 (2017).
- [38] See Supplemental Material at <http://link.aps.org/supplemental/10.1103/PhysRevX.13.011046> for more details about materials, methods and analysis.
- [39] Y. P. Pan, S. Y. Wang, X. Y. Liu, Y. S. Lin, L. X. Ma, Y. Feng, Z. Wang, L. Chen, and Y. H. Wang, *3D Nano-Bridge-Based SQUID Susceptometers for Scanning Magnetic Imaging of Quantum Materials*, *Nanotechnology* **30**, 305303 (2019).
- [40] Y. Li *et al.*, *Electronic Properties of the Bulk and Surface States of $\text{Fe}_{1+y}\text{Te}_{1-x}\text{Se}_x$* , *Nat. Mater.* **20**, 1221 (2021).
- [41] D. Golubchik, E. Polturak, and G. Koren, *Evidence for Long-Range Correlations within Arrays of Spontaneously Created Magnetic Vortices in a Nb Thin-Film Superconductor*, *Phys. Rev. Lett.* **104**, 247002 (2010).
- [42] J. Y. Ge, J. Gutierrez, V. N. Gladilin, J. T. Devreese, and V. V. Moshchalkov, *Bound Vortex Dipoles Generated at Pinning Centres by Meissner Current*, *Nat. Commun.* **6**, 6573 (2015).
- [43] L. Embon *et al.*, *Imaging of Super-Fast Dynamics and Flow Instabilities of Superconducting Vortices*, *Nat. Commun.* **8**, 85 (2017).
- [44] E. H. Brandt, *The Flux-Line Lattice in Superconductors*, *Rep. Prog. Phys.* **58**, 1465 (1995).
- [45] H. Ru, Y.-S. Lin, Y.-C. Chen, Y. Feng, and Y.-H. Wang, *Observation of Two-Level Critical State in the Superconducting FeTe Thin Films*, *Chin. Phys. Lett.* **36**, 077402 (2019).
- [46] W.-K. Kwok, U. Welp, A. Glatz, A. E. Koshelev, K. J. Kihlstrom, and G. W. Crabtree, *Vortices in High-Performance High-Temperature Superconductors*, *Rep. Prog. Phys.* **79**, 116501 (2016).
- [47] B. Kalisky, J. R. Kirtley, J. G. Analytis, J.-H. Chu, I. R. Fisher, and K. A. Moler, *Behavior of Vortices Near Twin Boundaries in Underdoped $\text{Ba}(\text{Fe}_{1-x}\text{Co}_x)_2\text{As}_2$* , *Phys. Rev. B* **83**, 064511 (2011).
- [48] I. M. Miron, K. Garello, G. Gaudin, P.-J. Zermatten, M. V. Costache, S. Auffret, S. Bandiera, B. Rodmacq, A. Schuhl, and P. Gambardella, *Perpendicular Switching of a Single Ferromagnetic Layer Induced by In-Plane Current Injection*, *Nature (London)* **476**, 189 (2011).
- [49] L. Liu, C.-F. Pai, Y. Li, H. W. Tseng, D. C. Ralph, and R. A. Buhrman, *Spin-Torque Switching with the Giant Spin Hall Effect of Tantalum*, *Science* **336**, 5 (2012).
- [50] V. Thampy, J. Kang, J. A. Rodriguez-Rivera, W. Bao, A. T. Savici, J. Hu, T. J. Liu, B. Qian, D. Fobes, Z. Q. Mao *et al.*, *Friedel-like Oscillations from Interstitial Iron in Superconducting $\text{Fe}_{1+y}\text{Te}_{0.62}\text{Se}_{0.38}$* , *Phys. Rev. Lett.* **108**, 107002 (2012).
- [51] Q. Liu, C.-X. Liu, C. Xu, X.-L. Qi, and S.-C. Zhang, *Magnetic Impurities on the Surface of a Topological Insulator*, *Phys. Rev. Lett.* **102**, 156603 (2009).
- [52] N. J. McLaughlin *et al.*, *Strong Correlation between Superconductivity and Ferromagnetism in an Fe-Chalcogenide Superconductor*, *Nano Lett.* **21**, 7277 (2021).
- [53] N. Zaki, G. Gu, A. Tsvelik, C. Wu, and P. D. Johnson, *Time-Reversal Symmetry Breaking in the Fe-Chalcogenide Superconductors*, *Proc. Natl. Acad. Sci. U.S.A.* **118**, 1 (2021).
- [54] C. Nayak, S. H. Simon, A. Stern, M. Freedman, and S. Das Sarma, *Non-Abelian Anyons and Topological Quantum Computation*, *Rev. Mod. Phys.* **80**, 1083 (2008).
- [55] C. Beenakker, *Search for Non-Abelian Majorana Braiding Statistics in Superconductors*, *SciPost Phys. Lect. Notes* **15** (2020), <https://scipost.org/SciPostPhysLectNotes.15>.
- [56] D. A. Ivanov, *Non-Abelian Statistics of Half-Quantum Vortices in p -Wave Superconductors*, *Phys. Rev. Lett.* **86**, 268 (2001).
- [57] A. Y. Kitaev, *Fault-Tolerant Quantum Computation by Anyons*, *Ann. Phys. (Amsterdam)* **303**, 2 (2003).
- [58] J. Alicea, *New Directions in the Pursuit of Majorana Fermions in Solid State Systems*, *Rep. Prog. Phys.* **75**, 076501 (2012).
- [59] J. Linder and A. V. Balatsky, *Odd-Frequency Superconductivity*, *Rev. Mod. Phys.* **91**, 045005 (2019).